Environmental Science and Pollution Research (2025) 32:9103–9124
https://doi.org/10.1007/s11356-025-36245-2

RESEARCH ARTICLE

Transmission of aerosols inside a moving auto rickshaw: a computational fluid dynamic study

Nirvik Sen[1] · **Krishna Kumar Singh**[1]

Received: 12 June 2024 / Accepted: 4 March 2025 / Published online: 19 March 2025

Abstract

We report a 3D Euler-Lagrangian CFD model to quantify the dispersion and transport of aerosols in a moving, semi-open auto rickshaw. The vehicle has a driver at the front, with two passengers seated behind in the rear section. This mode of transport is commonly seen in developing countries across Asia and Africa. Aerosol particles are generated due to the continuous, unmasked speaking of a passenger inside the auto rickshaw. The Eulerian portion of the model has been validated against reported experimental data on flow fields in enclosures with and without obstacles. Three RANS-based turbulence models—standard k-ε, realizable k-ε, and SST k-ω—are compared with experimental data, and the standard k-ε model is found to be the most suitable. Since the sides of the auto rickshaw are open, there is significant air exchange with the surroundings, which greatly affects the spread of aerosol particles. The presence of a partition between the driver and the passenger compartment reduces the probability of infection transmission from 1 to 0. A decrease in the auto rickshaw's speed from 60 to 20 km/h also reduces the probability of spread from 1 to 0. Additionally, a lateral wind (perpendicular or oblique to the direction of travel) further decreases the probability of transmission from 1 to 0. For all cases, the face velocity for all passengers is computed. The state of dispersion is significantly influenced by the location of aerosol generation. The relative importance of the different scenarios studied is quantified. Finally, a set of recommendations is outlined and compared with those reported for other modes of public transport.

Keywords Auto rickshaw · CFD · COVID-19 · Respiratory aerosols

Introduction

COVID-19 is arguably the most severe crisis the world has faced in at least four generations. As of October 2024, it has killed over 7.01 million people and infected over 704 million (Worldometer 2023). In early phase of the disease, COVID-10 had a case fatality rate (CFR) of ~ 20% of all hospitalized cases (Wang et al. 2023). As the virus mutated evolving over time into Omicron variant, CFR reduced significantly by as much as 96.8% (Horita and Fukumoto 2023). However, the variant was more contagious and overwhelmed containment strategies in densely populated parts of the world (Xu et al. 2023). Like its predecessor variant, Omicron also spread through transport of aerosols and was airborne (Wong et al. 2022). If anything the entire world had united upon for once, it is the urge to defend mankind form this disease.

Apart from the extensive research efforts in medicine, virology, and healthcare, significant work has also been conducted to understand how COVID-19 transmits and infects. It is well established that the primary mode of COVID-19 transmission is through aerosols and droplets expelled when an infected person sneezes, coughs, speaks, or sings. Tracking the movement of virus-laden aerosols in enclosed spaces such as rooms, classrooms, and hospital wards is a complex fluid dynamics problem, as droplet dispersion depends on airflow patterns within the space. Furthermore, these droplets evaporate over time, leaving behind tiny nuclei that, due to their extremely small size, can remain airborne for a significant duration (Liu et al. 2017). Computational fluid dynamics (CFD) simulations are instrumental in analyzing the spread of droplets and aerosols in different environments. Numerous studies have been conducted in this area. For instance, Ji and colleagues simulated the dispersion of

Responsible Editor: Philippe Garrigues

✉ Nirvik Sen
nirvik@barc.gov.in

[1] Chemical Engineering Division, Bhabha Atomic Research Centre, Trombay, Mumbai 400085, India

tiny droplets in a room with different ventilation systems (Ji et al. 2018). Dbouk and Drikakis simulated the spread of tiny droplets generated by a coughing event in an open environment under different wind and relative humidity conditions (Dbouk and Drikakis 2020a). Subsequently, the same researchers conducted similar simulations while considering the effect of a face mask worn by the coughing individual (Dbouk and Drikakis 2020b). Li and colleagues modeled the dispersion of tiny droplets while accounting for differences in humidity between exhaled and environmental air, assuming quiescent air conditions (Li et al. 2018). Sen performed numerical simulations to examine the spread of droplets produced by a coughing event inside an elevator (Sen 2021). Sen and Singh further reported numerical simulations of droplet transmission and evaporation during doorstep interactions between two individuals under varying wind and ventilation conditions near the door (Sen and Singh 2021a). The efficacy of face masks in preventing the spread of cough droplets inside a room has been evaluated using a 3D CFD model (Liu et al. 2022). Additionally, improved droplet dispersion inside a hospital ward in the presence of ventilation has been analyzed using a 3D CFD model (Song et al. 2023). In the above studies, the evaporation of the liquid component of cough droplets was considered. However, since the liquid content evaporates quickly, what remains are micron-sized nuclei. These tiny particles or aerosols can be transported over long distances by ambient airflow. Several studies have focused on the transport of such aerosols in different scenarios. Won and colleagues developed a CFD model to study the impact of room airflow on the performance of an upper-room UV germicidal irradiation system (Won et al. 2023). Saw and colleagues reported a CFD model predicting aerosol transport inside a hospital ward under different exhalation scenarios and varying chilled air supply rates (Saw et al. 2021). A comprehensive review on the dispersion mechanisms of virus-laden aerosols inside a hospital ward, along with various numerical approaches for their quantification, has also been published (Tan et al. 2022). The authors used a Lagrangian approach to track aerosol particles. A CFD-based study quantified aerosol transport inside a three-dimensional classroom, demonstrating how air purifiers can help reduce transmission risks (Abuhegazy et al. 2020). The transport and dispersion of virus-laden aerosols inside an air-conditioned restaurant have also been simulated, where turbulence in the computational domain was modeled using the LES technique (Liu et al. 2021). Similarly, a 3D CFD model was used to study aerosol transmission and dispersion inside a music classroom, revealing how air purifier placement and aerosol generation rates influence dispersion patterns (Narayanan and Yang 2021). The effect of fresh air exchange rates on the dispersion and spread of virus-laden aerosols inside underground metro passenger wagons has also been investigated (El-Salamony et al. 2021).

Studies on the spread of droplets and aerosols inside various modes of public transport have also been reported. Yang and colleagues simulated the transmission of evaporating micron-sized cough droplets inside an air-conditioned coach bus (Yang et al. 2020). Zhang and Li examined the spread and dispersion of cough droplets inside a high-speed rail cabin, which was also air-conditioned (Zhang and Li 2012). A CFD model was developed to quantify the dispersion and spread of airborne contaminants inside a passenger aircraft cabin during the ascent phase of flight (Elmaghraby et al. 2020). Similarly, Talaat and colleagues used a CFD model to study aerosol transport inside a Boeing 737 aircraft (Talaat et al. 2021). The spread of coronavirus-laden aerosol particles inside a poorly ventilated car was simulated using a 3D CFD model (Sarhan et al. 2022). The study found that in such an environment, it takes approximately 6.38 min for an infected driver to transmit the virus to passengers. Additionally, airflow patterns inside aircraft cabins and the distribution of vortices in long, narrow confined spaces, such as airplane cabins, have been analyzed. Mboreha and colleagues proposed a novel personalized ventilation system for aircraft to reduce the dispersion and spread of virus-laden particles (Mboreha et al. 2022). In all these cases, the vehicles were air-conditioned, meaning there was no exchange of air with the external environment. While numerous studies have used CFD to predict the dispersion and transmission of aerosols (as well as evaporating droplets) in public transport settings, nearly all of them have focused on enclosed, air-conditioned environments.

Mathai and colleagues developed a CFD model incorporating a species transport equation to predict the spread of pathogenic aerosols inside a car (Mathai et al. 2021). They modeled two individuals seated diagonally opposite each other and examined the effect of opening the windows on aerosol transmission. More recently, we reported an Euler-Lagrangian CFD model to quantify aerosol transmission and dispersion inside a moving sports utility vehicle (SUV) with open windows, allowing for air exchange between the vehicle's interior and the external environment (Sen and Singh 2021b).

In this study, we analyze the transmission of droplet nuclei (post-evaporation) inside a moving auto rickshaw—a common mode of transport in many Asian (including India) and African countries. The majority of research on aerosol transmission has focused on air-conditioned transportation systems such as trains, buses, aircraft, and cars. However, to the best of our knowledge, no study in the open literature has investigated a transport mode as simple and widespread as the auto rickshaw. Auto rickshaws are primarily used in densely populated countries where medical infrastructure is often limited. Therefore, understanding the mechanisms of aerosol transport and dispersion in such commonly used vehicles is crucial. This study aims to address this research

gap. While extensive research has been conducted on droplet and aerosol transport in enclosed, controlled environments, our work is the first to examine aerosol dispersion inside a semi-open auto rickshaw. This novelty forms the key contribution of our study. We consider an auto rickshaw with a semi-open configuration that allows significant air exchange with the surroundings. The study focuses on how aerosol dispersion is influenced by this continuous exchange of air between the interior of the auto rickshaw and the external environment. Unlike air-conditioned trains, buses, and aircraft, the interior of an auto rickshaw is not isolated; instead, air flows freely in and out. Understanding this interaction is essential for evaluating the potential spread of airborne pathogens in such transport settings.

The objective of this study is to understand how tiny aerosols disperse inside a moving auto rickshaw carrying one driver and two passengers seated in the back row. The airflow inside and outside the rickshaw is captured using a 3D Eulerian approach, while aerosol dispersion—resulting from one of the three individuals speaking—is modeled in a Lagrangian frame. It is assumed that aerosols (micron-sized nuclei) are generated due to continuous, unhindered speech by the driver or one of the two unmasked passengers seated behind. Aerosol ejection occurs in a horizontal plane, with a fixed particle diameter. The evaporation of the water fraction is not modeled, as it occurs on a timescale much smaller than the subsequent dispersion of the resultant aerosol particles. We compare two scenarios: one with a partition between the driver and passenger compartments and one without. Additionally, we examine the effects of vehicle speed, the location of the aerosol source, and the influence of lateral wind gusts on aerosol transport. The probability of infection spread is quantified for all cases. Finally, we propose a set of recommendations to minimize infection transmission in a moving auto rickshaw and compare our findings with observations reported for other modes of public transport.

Numerical model

Computational domain

Figure 1 illustrates the computational domain used in this study. The model considers a three-seater auto rickshaw with separate driver and passenger compartments. The sides of the auto rickshaw are completely open, allowing for significant air exchange with the surroundings. The computational domain includes both the vehicle and a portion of its surrounding environment. The surrounding enclosure is a rectangular box with dimensions $8 \times 5 \times 3$ m, which is larger than the vehicle itself. It is worth noting that the length of the surrounding enclosure considered in this study is shorter—particularly downstream of the vehicle—than what is typically required for estimating a vehicle's drag coefficient. In such cases, it is crucial to capture the entire length scale of eddies generated in the wake of the vehicle. However, in this study, our primary focus is on tracking aerosol dispersion in and around the auto rickshaw rather than evaluating aerodynamic drag. The auto rickshaw is assumed to be traveling in a straight path without taking any turns. The driver is centrally positioned in the driver's compartment, while two passengers are seated in the passenger compartment. To maintain computational efficiency, a simplified human body representation (in a seated posture) has been used. A rectangular mouth opening has been modeled based on the approach used in previous studies (Dbouk and Drikakis 2020a, 2020b). Two different geometrical configurations are analyzed: one with a partition between the driver and passenger compartments and one without.

Governing equations, initial and boundary conditions

An Euler-Lagrangian approach is used in this study. The airflow inside and outside the auto rickshaw is first modeled in an Eulerian reference frame. As the auto rickshaw moves forward at a finite speed, boundary layer separation occurs, generating eddies that facilitate significant air exchange between the interior and exterior of the vehicle. Turbulence within the computational domain is captured using the Reynolds-Averaged Navier–Stokes (RANS) approach. Although RANS-based turbulence modeling is simpler compared to more advanced techniques such as Large Eddy Simulation (LES) or Direct Numerical Simulation (DNS), it has been widely validated and proven effective for a broad range of practical applications with reasonably good accuracy (Baker et al. 2023).

Table 1 lists the governing equations used in this work. The Eulerian solution is arrived by solving conservation of mass and conservation of momentum equation (Eqs. 1 and 2 in Table 1). Turbulent shear stress term ($\overline{\tau}$) required for closure is dependent on turbulent viscosity (μ_T). μ_T is dependent on local values of turbulent kinetic (k) and dissipation rates (ε). In order to estimate the values of k and ε, separate conservation equations for k and ε are solved (Eqs. 4 and 5). Though three different RANS turbulence models are tested in this work, equations shown in Table 1 are that of standard k-ε model as it is seen to outperform others ("Validation of computational approach" section). Solution of Eqs. (1)–(7) generates the steady-state flow field in the enclosure around the auto rickshaw. Once the flow field is established for a given scenario, the micron-size aerosols are injected into the computational domain. These aerosols generated due to speaking of a person are treated as discrete particles using a Lagrangian approach. The spatial movement of aerosol particles due to prevailing

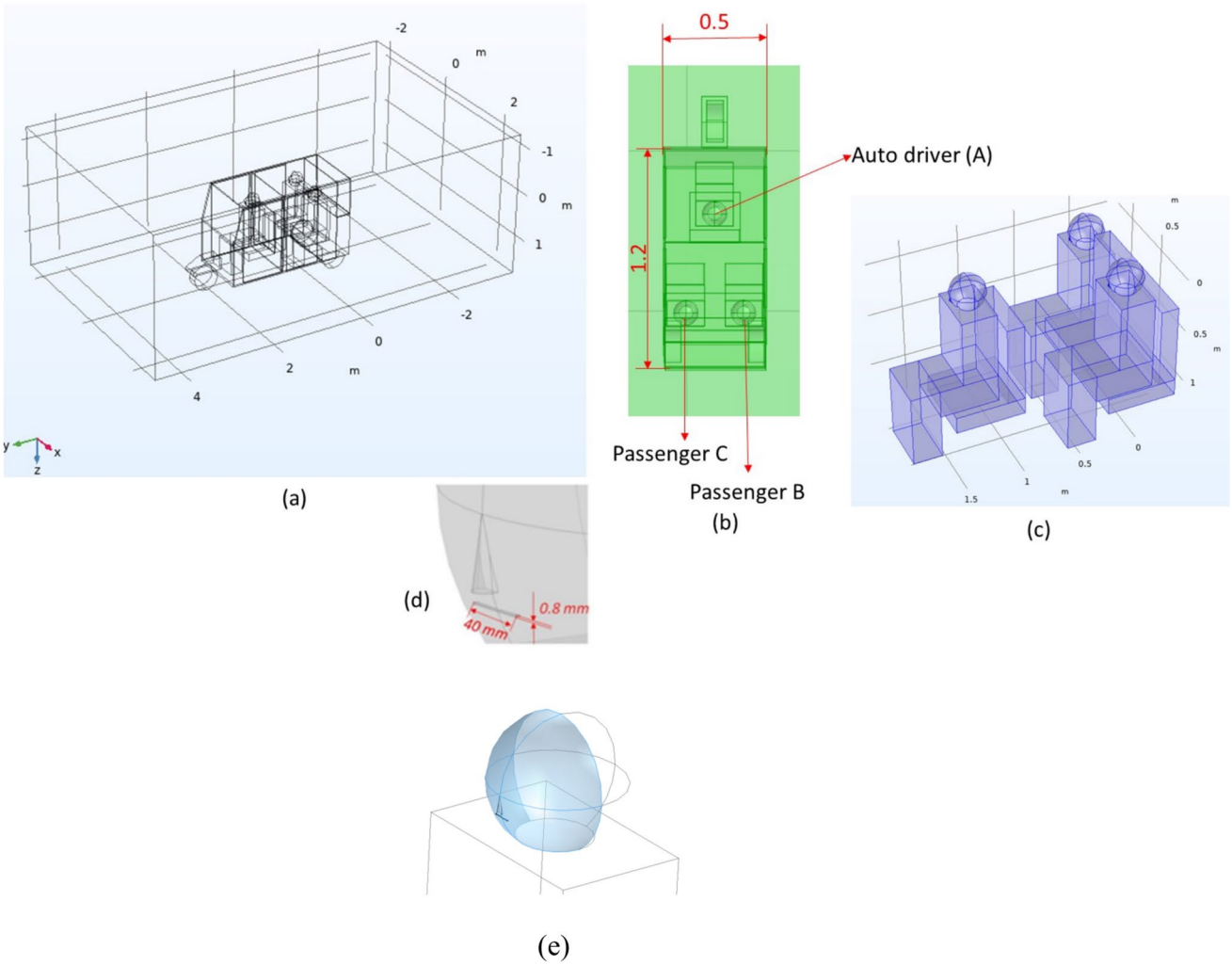

Fig. 1 A typical computational domain used in the numerical simulations. (**a**) shows the isometric view of the overall domain, (**b**) shows a part of the top view along with relevant dimensions, (**c**) shows the isometric view of the seating arrangement along with passengers in the auto rickshaw, (**d**) shows close-up of the face of a passenger a slit on which is used to define inlet boundary for aerosols, and (**e**) region of face considered for calculation of face-averaged velocity

Table 1 The governing equations solved

$\nabla.(\vec{u}) = 0$	Continuity equation	(1)
$\rho\frac{\partial\vec{u}}{\partial t} + \rho(\vec{u}.\nabla)\vec{u} = \nabla.\left[-pI + \overline{\overline{\tau}}\right] + \rho_c\vec{g}$	Momentum equation	(2)
$\overline{\overline{\tau}} = (\mu + \mu_T)\nabla\vec{u} + (\nabla\vec{u})^T$	Closure equation for momentum equation	(3)
$\frac{\partial}{\partial t}(\rho k) + \nabla.(\rho\vec{u}k) = \nabla.\left(\frac{\mu_t}{\sigma_k}\nabla k\right) + G_k - \rho\varepsilon$	Conservation of turbulent kinetic energy (k)	(4)
$\frac{\partial}{\partial t}(\rho\varepsilon) + \nabla.(\rho\vec{u}\varepsilon) = \nabla.\left(\frac{\mu_t}{\sigma_\varepsilon}\nabla\varepsilon\right) + \frac{\varepsilon}{k}(C_{1\varepsilon}G_k - C_{2\varepsilon}\rho\varepsilon)$	Conservation of turbulent energy dissipation rate (ε)	(5)
$\mu_t = \rho C_\mu\frac{k^2}{\varepsilon}\quad C_\mu = 0.09$	Closure to Eq. (4) and (5): turbulent viscosity term	(6)
$G_k = \mu_t\left(\nabla\vec{u} + \nabla\vec{u}^T\right) : \nabla\vec{u}$	Closure to Eq. (4) and (5): generation of turbulent kinetics energy	(7)
$m_d\frac{d\vec{u_d}}{dt} = (\rho_d - \rho)g + \frac{C_D\pi d_d^2\rho}{8}\lvert\vec{u_d} - \vec{u}\rvert(\vec{u_d} - \vec{u})$	Equation of motion of drop	(8)
$C_d = max\left\{\frac{24}{Re_d}(1 + 0.15Re_d^{0.687});0.44\right\}$	Closure to Eq. (8); Drag law	(9)

aerodynamics is captured by integrating the equation of motion of each particle (Eq. 8 in Table 1). The velocity field ($\vec{u}$) used in Eq. (8) is obtained from solution of Eqs. (1)–(7) (one-way coupling). In Eq. (8), $m_d \frac{d\vec{u_d}}{dt}$ represents particle acceleration. The term $\left(\rho_d - \rho\right)g$ is the gravitation force acting on the particles while $\frac{C_D \pi d_d^2 \rho}{8}\left|\vec{u_d} - \vec{u}\right|\left(\vec{u_d} - \vec{u}\right)$ represents the drag force acting on the particles. Drag force has been quantified using Schiller–Naumann drag law (Sen 2021; Sen and Singh 2021a) and is shown in Table 1 as Eq. (9).

Density and viscosity of continuous medium (air) used in Eulerian part of the simulation are considered to be 1.19 kg/m^3 and 0.018 cP, respectively. Mouth of a person is modeled as a rectangular slit (Dbouk and Drikakis 2020a). Diameter of the aerosol particles of interest are typically in the range of 1–10 µm (Narayanan and Yang 2021). We have considered a fixed aerosol particle diameter of 10 µm in this work. Evaporation of the liquid component of the ejected particle/drop is not modeled as time scale of evaporation is negligibly small compared to that of resultant aerosol nuclei. Only one-way coupling between the Lagrangian particles and the Eulerian flow field is considered (Abuhegazy et al. 2020). The number density of particles coming out of the mouth while speaking is considered to be 570 particles per second (Narayanan and Yang 2021). The velocity with which these particles are ejected is considered to be 0.16 m/s (Narayanan and Yang 2021). Particle density is considered to be 1000 kg/m^3. This is because the aerosol essentially represent the remains (salt) of the respiratory droplets after complete and quick evaporation of the water content. After being released, these particles get entrained in the prevailing aerodynamics and spread across the computational domain. Drag force acting on the aerosols has been modeled using the law proposed by Schiller and Naumann (Eq. 9 in Table 1). Particles falling onto any surface get "trapped" on to the surface while a "disappear" boundary condition is defined at outflows.

Results and discussion

Grid independence test

The geometry of the auto rickshaw allows for significant exchange of mass and momentum between its interior and the surrounding environment. This interaction leads to boundary layer separation and the formation of vortices. To accurately capture these flow characteristics, a sufficiently refined mesh is required. It is essential to determine the optimal mesh density—one that is fine enough to resolve intricate flow details while avoiding excessive computational costs. To achieve this balance, four different mesh densities, ranging from 5829 to 26,454 cells/m^3, were tested. In all cases, refinements were applied near walls and sharp corners to enhance accuracy. The key parameter tracked for mesh validation was the velocity along line GG (a horizontal line spanning the width of the computational domain), as illustrated in Fig. 2.

Line GG is located just behind the driver's seat and was chosen due to the presence of sharp velocity gradients both inside and outside the rickshaw, as well as the formation of vortices. The results indicate that at lower grid densities (8529 and 10,750 cells/m^3), the vortices are not well resolved. Instead of capturing two distinct vortices, the simulation predicts a single merged vortex. However, for higher grid densities (15,707 and 26,454 cells/m^3), both vortices are accurately resolved, and the results are nearly identical. Additionally, the effect of grid refinement was analyzed along line HH (a horizontal line along the length of the computational domain) and line II (a vertical line passing through the passenger compartment). Across most regions, the local velocities predicted using a grid density of 15,707 cells/m^3 closely match those obtained with 26,454 cells/m^3, indicating that further refinement does not significantly alter the results. Thus, a grid density of 15,707 cells/m^3 is deemed sufficient and has been used for all simulations in this study.

To quantitatively validate the suitability of a grid density of 15,707 cells/m^3 in this study, we also estimated the Grid Convergence Index (GCI). The pressure drop across the front and rear surfaces of the auto rickshaw was measured at four different grid densities while keeping the vehicle speed fixed at 60 km/h and no partition between the driver and passenger compartments. The recorded pressure drop values were 143.271, 142.959, 144.61, and 144.663 Pa for grid densities of 8529, 10,750, 15,707, and 26,454 cells/m^3, respectively.

Using this data, GCI was calculated based on Eq. (10).

$$GCI(i+1,i) = \frac{F_s \epsilon_{rms(i+1,i)}}{r(i+1,i)^p - 1}$$
$$p\ (order\ of\ convergence) = \frac{\ln\left(\frac{O2-O1}{O3-O2}\right)}{\ln(r_{32})} \quad (10)$$

F_s is safety factor (taken as 1.25 here), $r(i+1,i)$ is refinement factor between one pair of grid density ($=N_{i+1}/N_i$), and $\epsilon_{rms}(i+1,i)$ is relative difference between the corresponding pressure drop values ($=\text{abs}(O_{i+1} - O_i)$). N_i and O_i are the grid density (cells/m^3) and computed pressure drop in i-th grid trail ($i = 1$, 2, and 3).

GCI for a grid refinement from 8529 to 10,750 cells/m^3 is 0.219 (21.93%). GCI for grid refinement from 10,750 to 15,707 cells/m^3 is 0.4775 (47.75%), while GCI for the final leg of refinement (i.e., 15,707 to 26,454 cells/m^3) is 0.007397 (0.739%) which quantitatively proves that a grid density of 10,750 cells/m^3 is sufficient as GCI for this refinement is less than 5%.

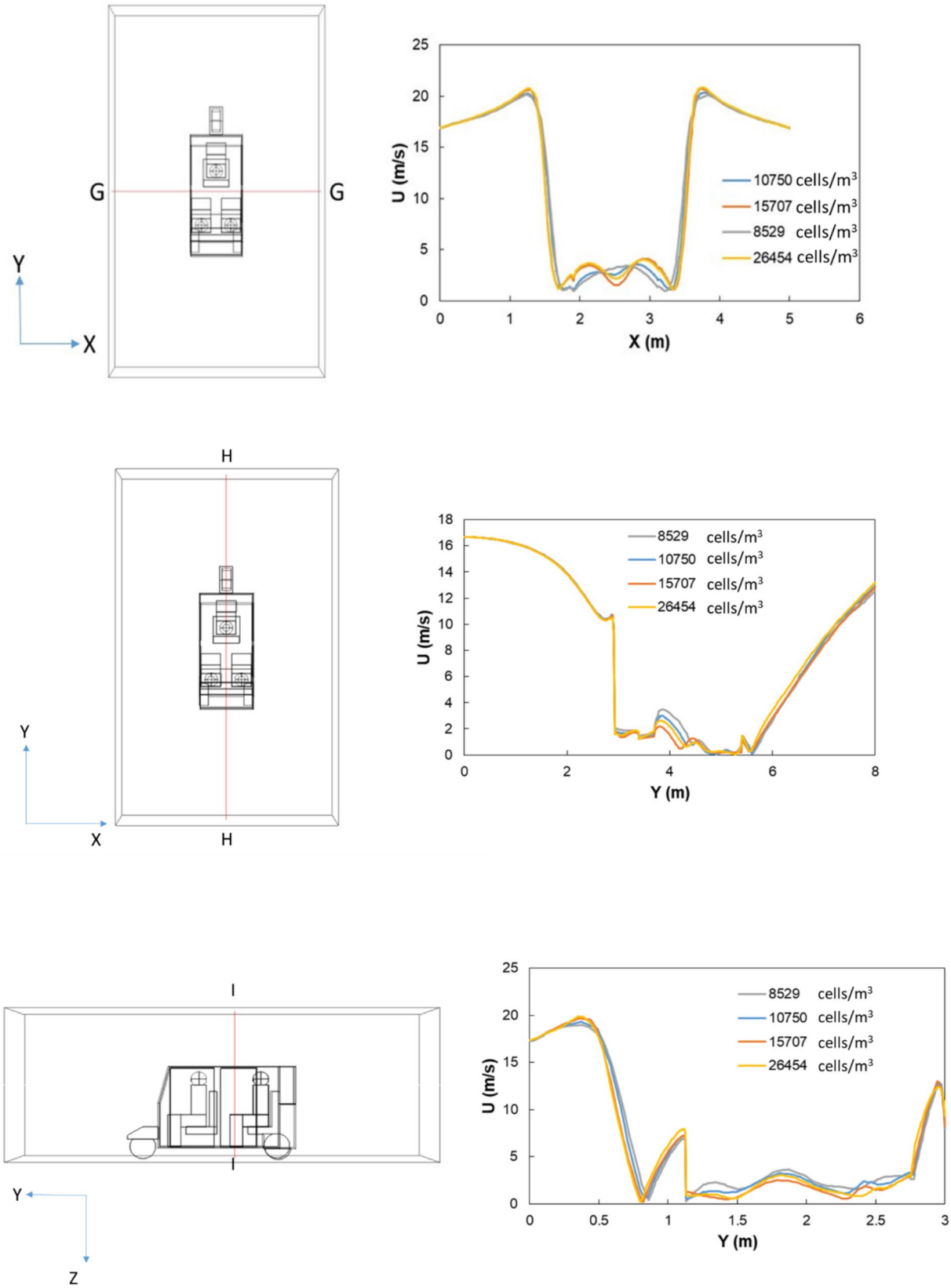

Fig. 2 Results of grid independence test

Validation of computational approach

In this section, we validate the accuracy of the CFD model by comparing its predictions of local velocity in a cubic enclosure with experimental data reported by Wang and Chen (2009). In their study, Wang and Chen used a cubical test room measuring $2.44 \times 2.44 \times 2.44$ m. Air entered the room through a full-width inlet slot (0.03 m wide) near the ceiling and exited through a full-width exhaust slot (0.08 m wide) near the floor on the opposite side. The supply air was delivered through a pressure plenum, ensuring a stable and uniform velocity across the entire width of the inlet slot. The airflow rate was 0.10 m^3/s. Local velocity measurements were taken at four different points inside the enclosure using ultrasonic anemometers. We have used this dataset to validate the predictive accuracy of our CFD model. Other researchers, such as Horikiri and Yao (2011), have also used this dataset to validate CFD simulations. The model replicates the exact room dimensions, including the precise locations of the inlet and exhaust slots. Figure 3a illustrates the geometry, the measurement points/lines, and the boundary conditions used in the simulations. Three different RANS-based turbulence

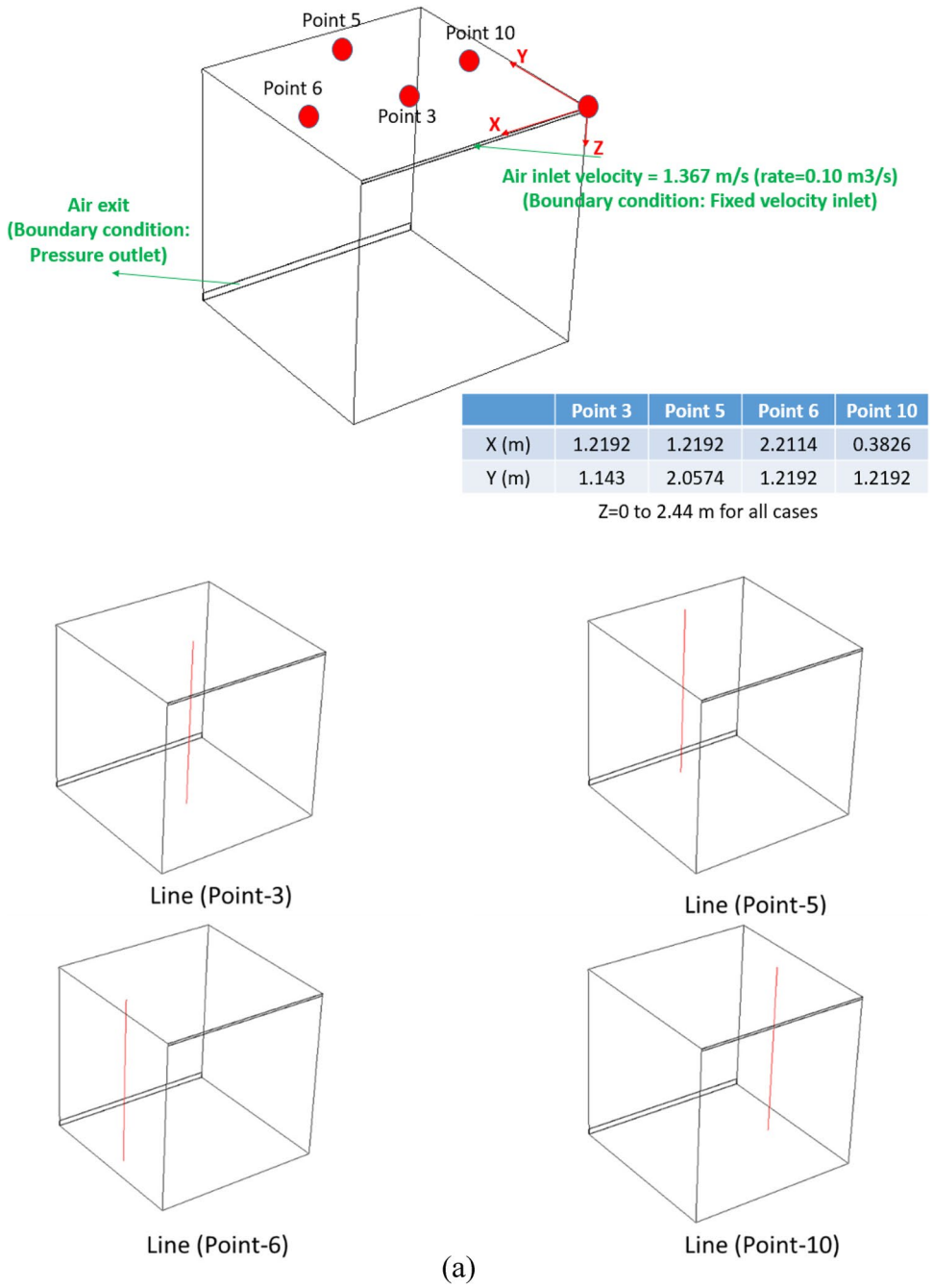

	Point 3	Point 5	Point 6	Point 10
X (m)	1.2192	1.2192	2.2114	0.3826
Y (m)	1.143	2.0574	1.2192	1.2192

Z=0 to 2.44 m for all cases

Fig. 3 **a** Computational domain showing four measurement locations. **b** Comparison of velocity profile predicted by CFD model against reported experimental data for points 3, 5, 6, and 10

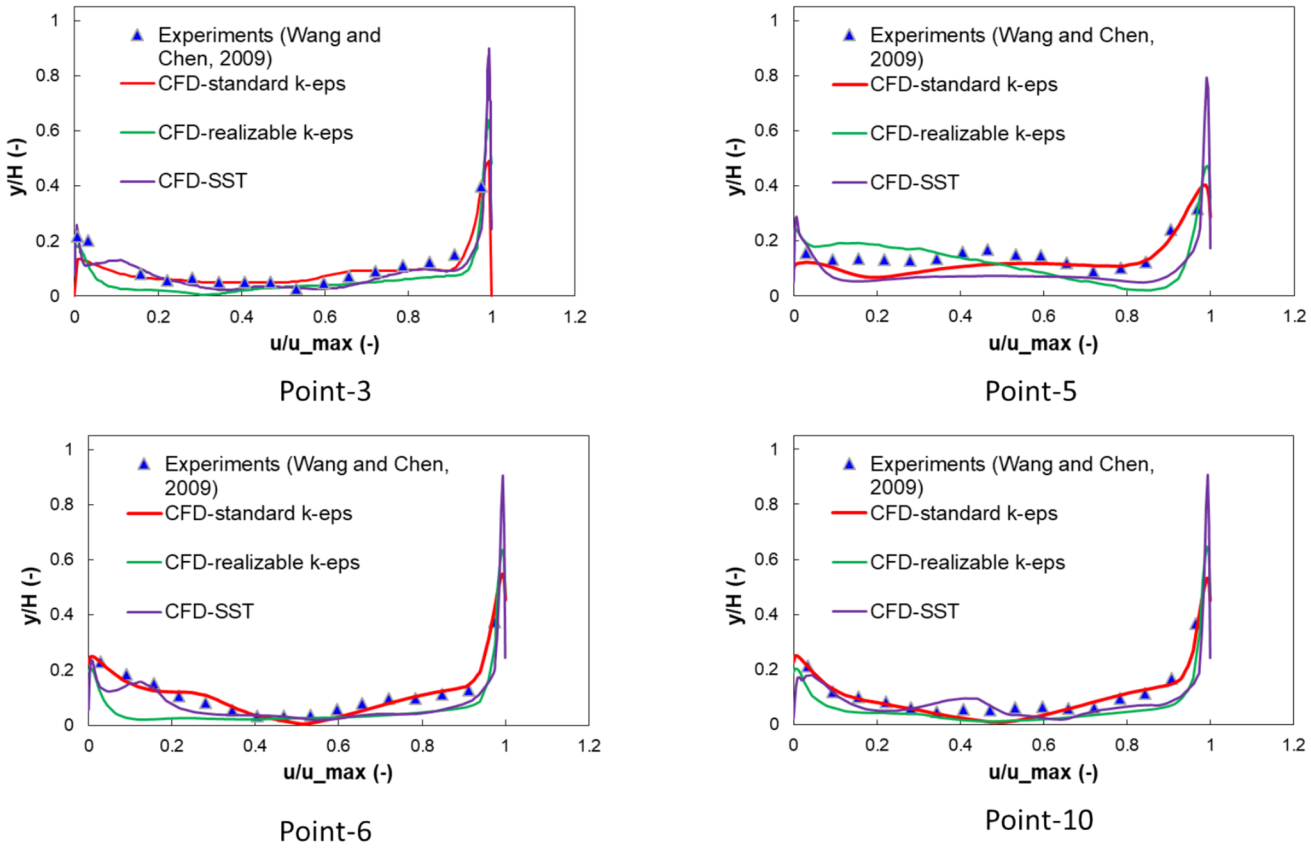

(b)

Fig. 3 (continued)

closure models, namely, standard k-ε, realization k-ε, and shear stress transport k-ω (SST k-ω) turbulence model, have been compared for their predictive ability.

As seen in Fig. 3b, the CFD-predicted velocity profile closely matches the experimental data, particularly for the classical standard k-ε model. This agreement is especially evident at points 6 and 10. The SST k-ω model also performs well, but its predictions exhibit oscillations in the velocity profile that are not observed in the experimental data (notably at points 6 and 10). On the other hand, the realizable k-ε model underpredicts local velocity at these points. The standard k-ε model also demonstrates strong performance for the other two measurement points. Based on this analysis, the classical standard k-ε model is chosen for further simulations. This study validates the reliability of CFD simulations in predicting the spread of respiratory aerosols inside and outside the auto rickshaw as considered in this work.

In addition to validating the flow field inside an empty enclosure with air inlet and exhaust, we present a second validation case where the modeled geometry includes a cubical object inside the enclosure. The presence of this 4×4×4 ft cube distorts the flow field and causes boundary layer separation. This scenario is separately reported by Wang and Chen (2009), who provide local velocity profiles at point 6, as illustrated in Fig. 4a. In our study, we simulate the movement of the auto rickshaw by modeling a static auto rickshaw inside an enclosure, with airflow directed through the domain to interact with the vehicle. This setup is conceptually similar to airflow within a box interacting with a centrally placed cube, as reported by Wang and Chen. The standard k-ε model is used to quantify turbulence parameters in this case. The results, shown in Fig. 4b, demonstrate a reasonably good agreement between the CFD-predicted velocity profile and the experimentally reported data (Wang and Chen 2009), further validating the suitability of our model for the current study.

Effect of partition between driver and passenger compartment

As mentioned earlier, two geometries are modeled—one where a barrier separates the driver compartment from the passenger compartment and another where no such barrier

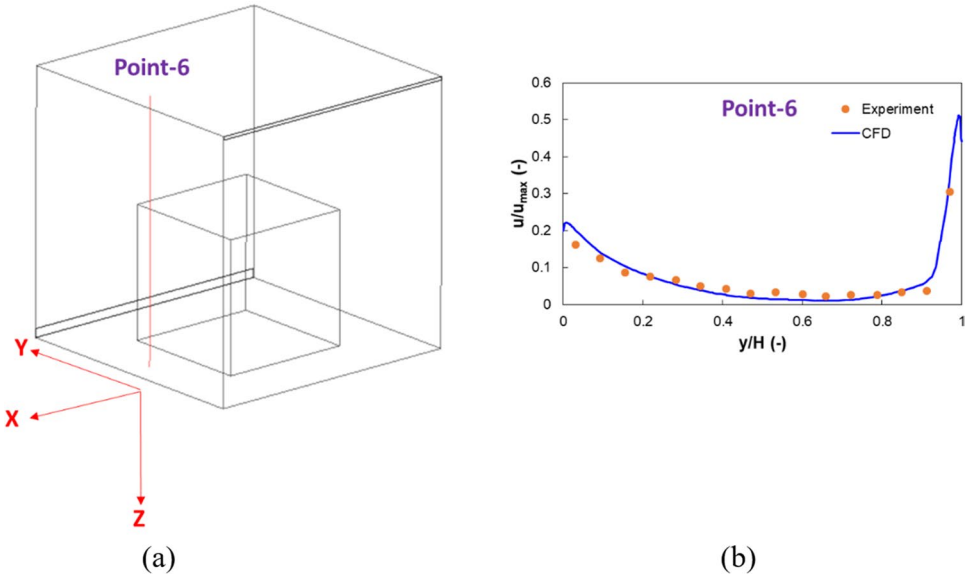

Fig. 4 **a** Computational domain showing the measurement location (point 6) and cube inside box configuration. **b** Comparison of velocity profile predicted by the CFD model against reported experimental data at point 6

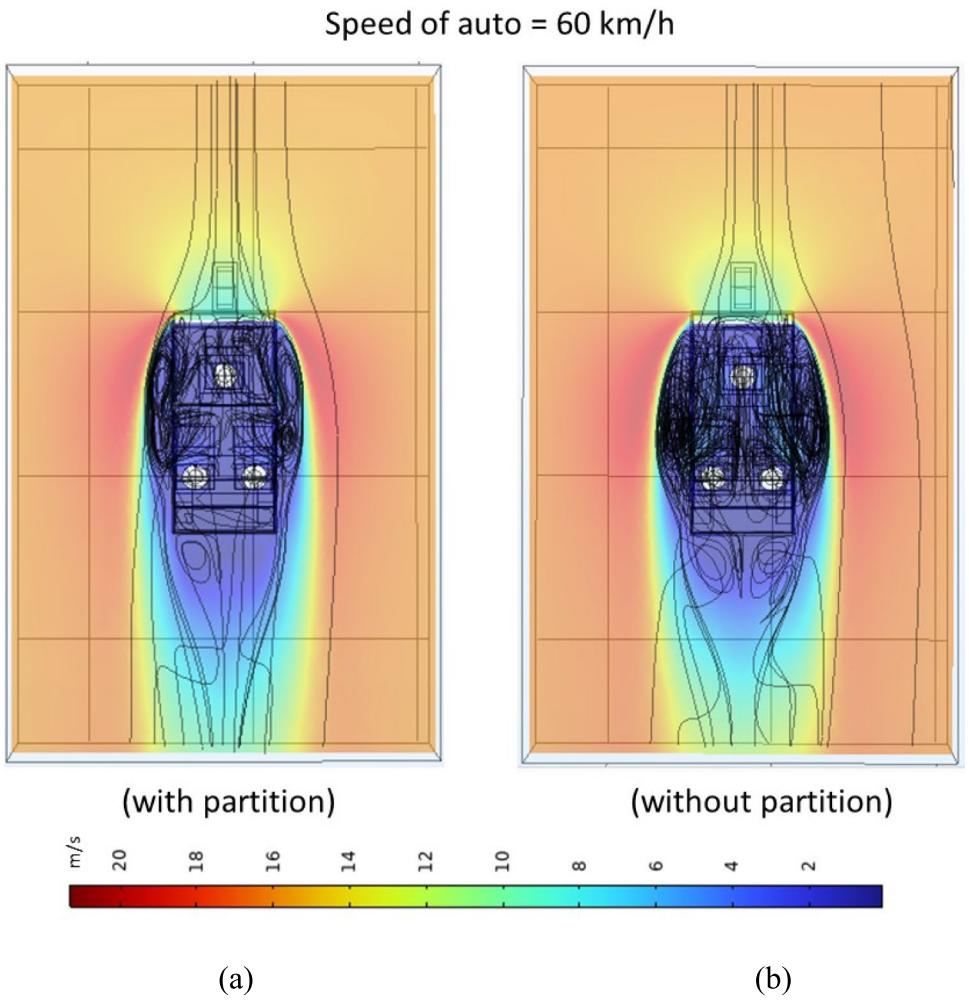

Fig. 5 Velocity contour with stream lines for an auto rickshaw **a** with and **b** without partition between driver and passenger compartments. Vehicle speed is 60 km/h. Color bar is in m/s

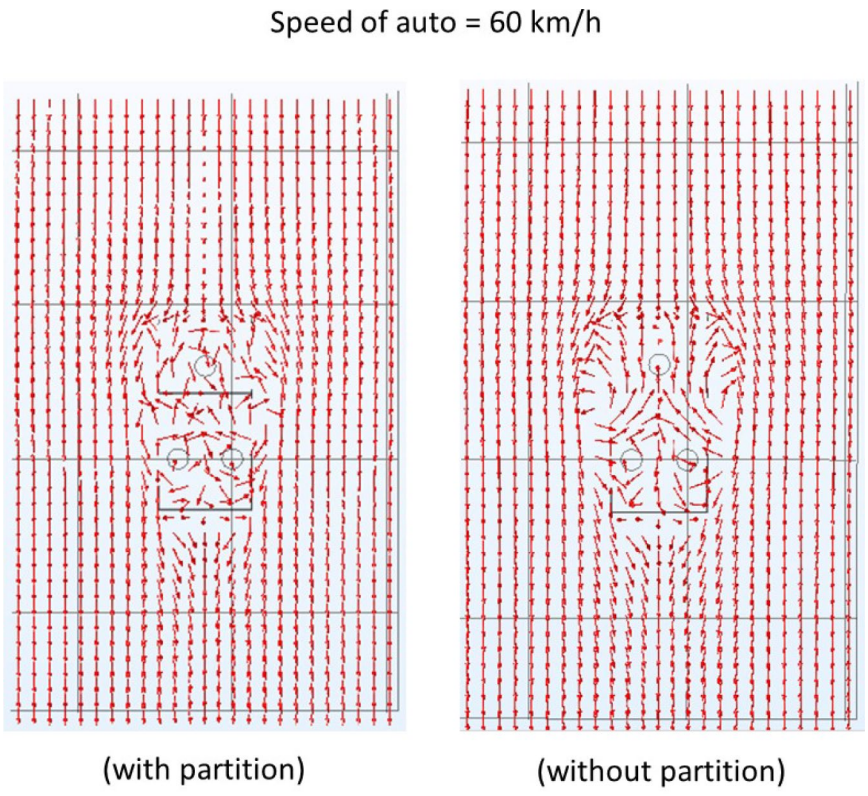
Speed of auto = 60 km/h
(with partition)
(without partition)

(a) (b)

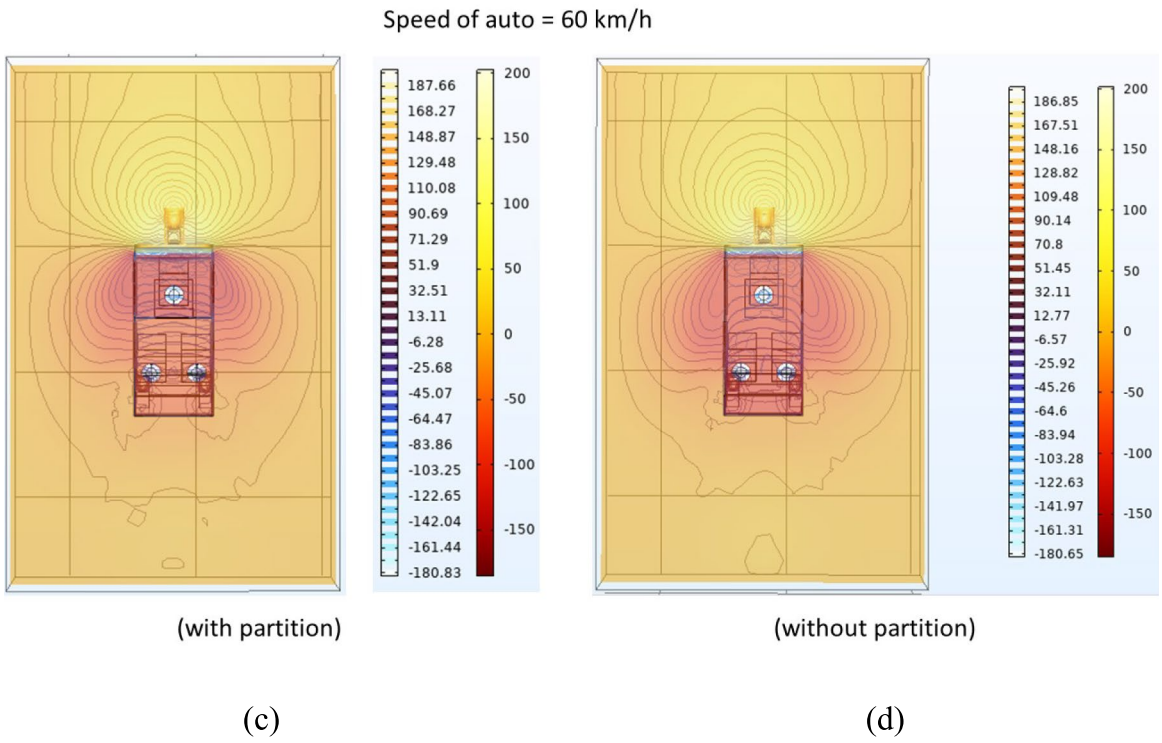
Speed of auto = 60 km/h
187.66
168.27
148.87
129.48
110.08
90.69
71.29
51.9
32.51
13.11
-6.28
-25.68
-45.07
-64.47
-83.86
-103.25
-122.65
-142.04
-161.44
-180.83
200
150
100
50
0
-50
-100
-150
186.85
167.51
148.16
128.82
109.48
90.14
70.8
51.45
32.11
12.77
-6.57
-25.92
-45.26
-64.6
-83.94
-103.28
-122.63
-141.97
-161.31
-180.65
(with partition)
(without partition)

(c) (d)

◂**Fig. 6** **a** Normalized velocity vector for moving auto rickshaw with partition, **b** normalized velocity vector for moving auto rickshaw without partition, **c** pressure contour and iso-contours for moving auto rickshaw with partition and **d** pressure contour and iso-contours for moving auto rickshaw without partition. Auto-rickshaw speed is 60 km/h. No lateral wind. Pressure contour/iso-contour color bar is in Pa

is present. Figure 5(a) and (b) displays the flow velocity contours along with streamlines for both cases (with and without a barrier). The contour plots (for velocity and pressure) are taken in a horizontal plane that aligns with the driver's mouth level.

The speed of the auto rickshaw is fixed at 60 km/h, which is reasonably high for roads in congested urban cities in Southeast Asia and Africa. As the auto rickshaw moves forward, the blunt surface of the vehicle (the windscreen) causes boundary layer separation. Due to this and the open framework of an auto rickshaw, there is significant air exchange between the interior and exterior. Comparing the streamlines in the two cases—with and without a partition—it is evident that in the absence of a partition, the streamlines extend more freely between the driver and passenger compartments. Figure 6(a–d) illustrates the normalized velocity vectors, pressure contours, and iso-pressure lines. The results are shown in a horizontal plane aligned with the driver's mouth level. The vector plot (Fig. 6(a–b)) clearly demonstrates that air mixes freely between the two compartments when no partition is present. Figure 6(c–d) shows that the windscreen increases pressure just in front of it, while a negative pressure region forms immediately behind it. This pressure difference drives airflow into the auto rickshaw. The pressure inside the passenger compartment is lower (more negative) when no partition is present compared to when one is installed. The predicted pressure drop across the front and rear surfaces of the auto rickshaw is 144.61 and 140.646 Pa for the cases without and with a partition, respectively. However, there is little difference in overall pressure drop across the vehicle. This is expected, as the partition affects the internal flow field but does not significantly alter the overall airflow around the auto rickshaw, as seen in Fig. 6(a–b).

Face-averaged velocities (calculated over the front half of the face, including the nose and mouth, as shown in Fig. 1) are also estimated from the model. For the case without a partition, the face-averaged velocities for passengers A, B, and C are 1.40, 0.76, and 0.88 m/s, respectively. When a partition is present between the driver and passenger compartments, the corresponding values are 1.13, 0.88, and 1.00 m/s for passengers A, B, and C, respectively. It is observed that the local face velocity decreases for the driver (passenger A) while it increases for passengers B and C when a partition is introduced. This occurs due to the altered internal airflow pattern created by the partition.

Now, suppose the driver in the auto rickshaw starts speaking without wearing a mask. Particles (10 μm in size) are generated at a rate of 570 particles per second (Narayanan and Yang 2021). These particles become entrained in the prevailing airflow and disperse throughout the compartments. Each passenger (excluding the speaking driver) is assigned a risk parameter. A passenger is considered "at risk" if any droplet is detected within an imaginary cubic enclosure with a 0.4-m edge length, centered on the spherical head of a seated human. This qualitative risk parameter is labeled "safe" if no micron-sized droplets enter the imaginary cube. However, if even one droplet enters this space at any point, the risk status changes to "at risk." Fig. 7 illustrates the spread of these potentially virus-laden particles inside the auto rickshaw. When a partition separates the driver and passenger compartments, the particles emitted by the driver remain circulating within the driver's compartment for some time before exiting the vehicle without reaching the passenger compartment. As a result, both passengers B and C remain safe (indicated in green). However, in the absence of a partition, the particles recirculate within both compartments, exposing both rear-seat passengers to potential risk. In this scenario, the passengers in the back seat are clearly not safe (indicated in red).

Effect of auto-rickshaw speed

In the previous section, we have seen that transmission of micro-droplets is rampant in case there is no partition between the driver and passenger compartment. The simulations are reported for a rather high speed (for auto rickshaws traveling in a city/urban setting). In this section, we simulate a condition wherein the speed of the auto rickshaw is reduced to 20 km/h. Such a scenario is quite common in traversing through crowded lanes/streets in an urban setting. Figure 8(a–b) shows the velocity contour with streamlines at a plane at the elevation of the driver's mouth (source of particles) for 20 and 60 km/h vehicle speed. Simulations are for the case of no partition between driver and passenger compartment. The results indicate that, for both speeds, the nature of boundary layer separation and vortex formation is similar. The vortices primarily form on either side of the auto-rickshaw frame, just behind the windshield, and extend across both the driver and passenger compartments. Although the axial span of the vortices is similar in both cases, the radial span is slightly smaller when the auto rickshaw is traveling at 20 km/h. This difference is clearly illustrated in Fig. 8(c–d), which present the pressure contour plot at the same plane. It can be observed that the extent of negative pressure inside both the driver and passenger compartments is significantly greater at the higher speed. Consequently, stronger winds rush inside with greater intensity, leading to a slightly larger radial span of the vortices. The

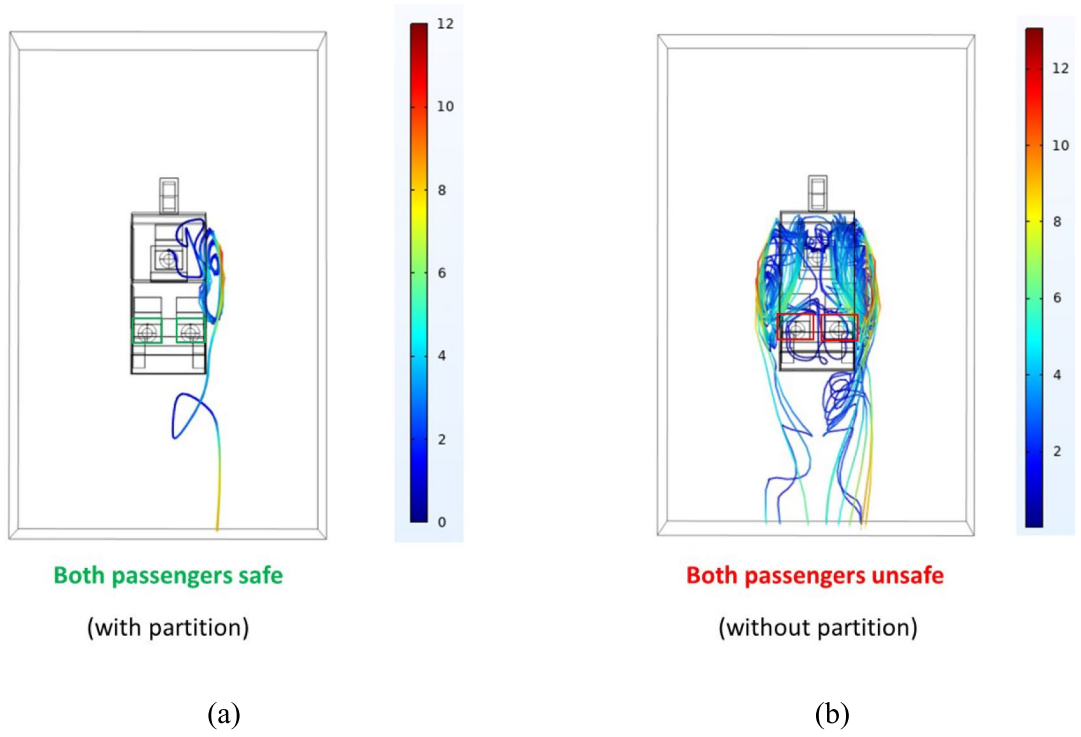

Fig. 7 Top view of aerosol particle tracks for **a** partition between driver and passenger compartments and **b** without a partition between driver and passenger compartments. Auto-rickshaw speed is 60 km/h. Color bar represents particle velocity in m/s

local flow velocity at each passenger's face was also calculated. At an auto-rickshaw speed of 20 km/h, the predicted velocities at the faces of passengers A, B, and C are 0.45, 0.23, and 0.27 m/s, respectively. In contrast, at 60 km/h, the corresponding values increase to 1.40, 0.76, and 0.88 m/s. This indicates that the local face velocities decrease as the vehicle speed is reduced. A decrease in the pressure differential across the lateral surfaces of the auto rickshaw (i.e., the regions through which external air enters), as seen in Fig. 8(c–d), contributes to the reduction in local face velocities at the lower speed of 20 km/h. Additionally, the pressure differential between the front and rear surfaces of the auto rickshaw is predicted to be 15.69 Pa at 20 km/h, whereas at 60 km/h, this value is significantly higher at 144.61 Pa.

Now, suppose the driver starts speaking without wearing a mask, thereby generating particles. Once again, these particles get caught in the prevailing flow field and spread throughout the auto rickshaw's interior. Since there is no partition, there is a possibility that the particles will reach the passenger compartments. Figure 9(a–d) illustrates what actually happens, with both top and side views provided. It is evident that when the auto rickshaw is moving at a low speed (20 km/h), the particles become trapped in the vortices but do not spread radially to an extent that endangers the passengers. Both passengers are marked safe. This is clearly due to the reduced radial span of the vortices generated at lower speeds. In contrast, at higher speeds (60 km/h), the particles penetrate deep into the passenger compartments and pass very close to the passengers, thereby posing a risk to their safety. This study, through CFD simulations, clearly demonstrates that it is advisable to travel at lower speeds unless a protective partition is in place between the driver and the passenger compartments.

Effect of gust of wind

In this section, we examine the effects of a lateral wind gust on the open lateral surfaces of a moving auto rickshaw. This represents a realistic scenario in which the wind blows in a direction perpendicular or oblique to the motion of the auto rickshaw. Figure 10(a–c) presents the velocity contours along with streamlines at a plane corresponding to the elevation of the driver's mouth (the source of particles).

The simulations are conducted for a case where there is no partition between the driver and passenger compartments, and the vehicle speed is maintained at 60 km/h. Two cases have been simulated. In the first case, a wind blowing at 20 km/h (a typical value in an urban setting) is directed perpendicular to the auto rickshaw's motion (Fig. 10b). In the second case, the wind, also blowing at 20 km/h, is oblique, making a 45-degree angle with the vehicle's direction of movement (Fig. 10c). This second scenario is particularly

relevant when the auto rickshaw takes a sharp turn, a common occurrence in urban environments. The results are compared with the case in which no wind is present (Fig. 10a).

The results indicate that boundary layer separation is completely altered in the presence of a lateral wind gust. When the auto rickshaw is traveling straight without any lateral wind, nearly equal-sized vortices form behind the windshield on either side of the vehicle (Fig. 10a). However, in the presence of a lateral wind gust (both perpendicular and oblique) at 25 km/h, a single vortex forms at the center of the driver's compartment (Fig. 10b, c). In this case, the streamlines exit through the right-hand lateral opening of the auto rickshaw due to the wind direction, which flows from left to right (top view). Additionally, a region of high velocity is observed when lateral wind is present (Fig. 10b, c). This occurs due to the interaction between two incoming air streams—the lateral wind gust and the airflow entering the auto rickshaw as a result of its motion.

The local flow velocity at the face of each passenger is also calculated. For a perpendicular lateral wind of 20 km/h, the predicted velocities at the faces of passengers A, B, and C are 1.30, 7.55, and 13.22 m/s, respectively. In the case of an oblique wind gust at 20 km/h, the corresponding values are 0.98, 9.19, and 15.03 m/s for passengers A, B, and C, respectively. These local velocity values are significantly higher than when there is no wind. This is because the lateral wind gust directly enters through the open sides of the auto rickshaw and interacts with the passengers, particularly passengers B and C, who are seated in the passenger compartment. In contrast, when there is no wind, the windshield of the auto rickshaw prevents direct interaction between the incoming head-on airflow and the driver or passengers. Additionally, the pressure differential between the front and rear surfaces of the auto rickshaw is 279.1 Pa for a perpendicular wind gust. The corresponding value for an oblique wind gust is 241.8 Pa.

Now, suppose the driver starts speaking without a mask, generating respiratory aerosols. The particles become entrained in the airflow and follow the flow field. Figure 11(a–f) illustrates the trajectory of these particles for two cases involving lateral wind, with both top (Fig. 11a–c) and side (Fig. 11d–f) views shown. The results indicate that in the presence of a lateral wind, the particles generated by the driver simply exit the auto rickshaw. In both cases—perpendicular wind and oblique wind at 20 km/h—none of the passengers seated behind the driver are affected. This occurs because the streamlines exit through the right-hand lateral opening of the auto rickshaw, as shown in Fig. 10. For the oblique wind case, the particles become temporarily trapped in a region above the driver's head, likely due to a local low-pressure zone. However, they eventually move out through the lateral opening of the auto rickshaw without coming close to passengers B and C. This study demonstrates that even a modest lateral wind blowing across a moving auto rickshaw significantly reduces the risk of infection spread. Such a scenario is typical for semi-open vehicles like the auto rickshaw considered in this work.

Effect of location of persons speaking

In the previous sections, we discussed what happens when the driver speaks continuously without a mask. In this section, we compare particle trajectories when one of the passengers speaks without a mask. Simulations are conducted to quantify particle spread when any of the three individuals in the auto rickshaw—the driver, passenger B, or passenger C—speaks without a mask. The results for two cases—an auto rickshaw traveling at 60 km/h with and without a partition—are summarized below. Figure 12(a–f) illustrates the spread of particles when a partition is present between the driver's and passengers' compartments.

The results show that when the driver speaks, the ejected aerosol particles become temporarily trapped in the vortices near the edge of the auto rickshaw before moving backward and exiting the enclosure without entering the passenger compartment. As a result, both passengers (B and C) remain unaffected. Similarly, when passenger C speaks, the particles move forward, become entrained in the vortex near the left-hand edge of the auto rickshaw, and then move backward and exit the enclosure. While following this trajectory, the particles do enter the driver's compartment but do not pass close to the imaginary cube centered around the driver's head (as seen in the side view). Consequently, the driver (A) remains safe. Additionally, the particles do not enter the passenger compartment on their way out, ensuring that both passenger B and the driver (A) are not exposed. However, when passenger B speaks, the particles move forward and become entrained in the prevailing vortex on the right-hand side. At this point, some particles move backward and exit the auto rickshaw enclosure following the existing flow field, while others are injected into the vortex on the opposite side of the auto rickshaw, directly across the driver's compartment. This complex trajectory causes some particles to pass very close to the driver and also enter the passenger compartment before exiting, potentially exposing passenger C to infection. Thus, in this case, both passenger C and the driver (A) are at risk. It is interesting to note the lack of symmetry in this case. Though passengers B and C are placed symmetrically with respect to the driver, the streamlines shown in Fig. 5 show that the vortices generated on either side of the auto rickshaw, though very similar, are not exactly identical. From a numerical perspective, this may be because of minute differences in the geometry tolerance (less than 0.001 m) or near wall meshing of the computational domain. However, this is a rather conservative picture of any real-life scenario where exact symmetry cannot be attained.

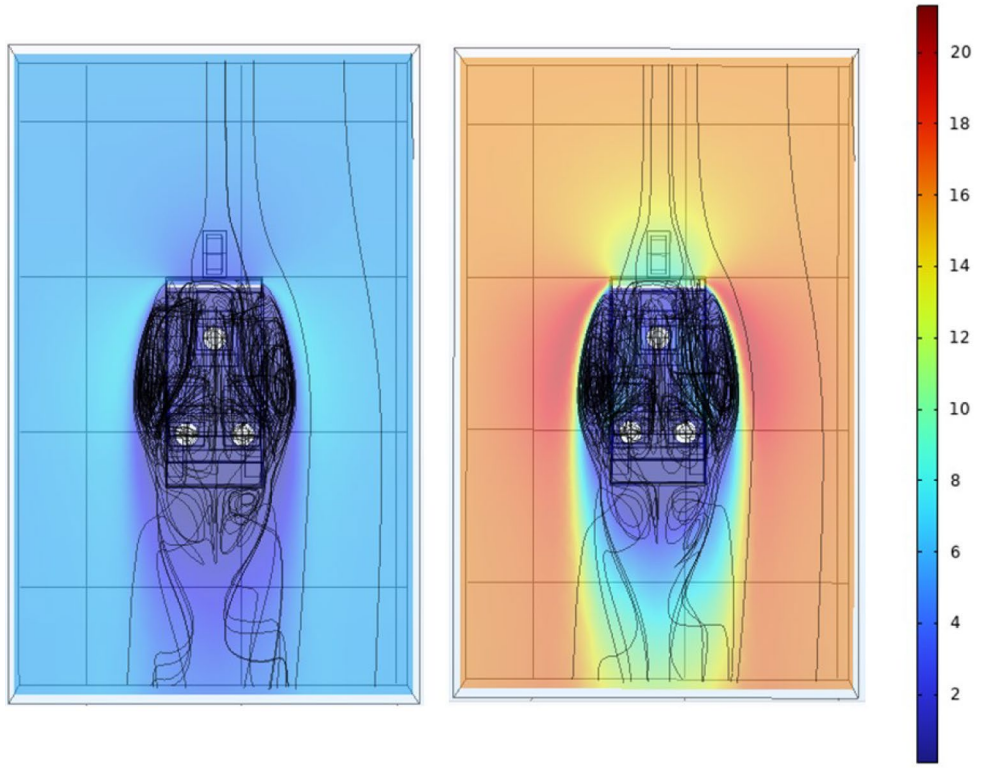

(a) (b)

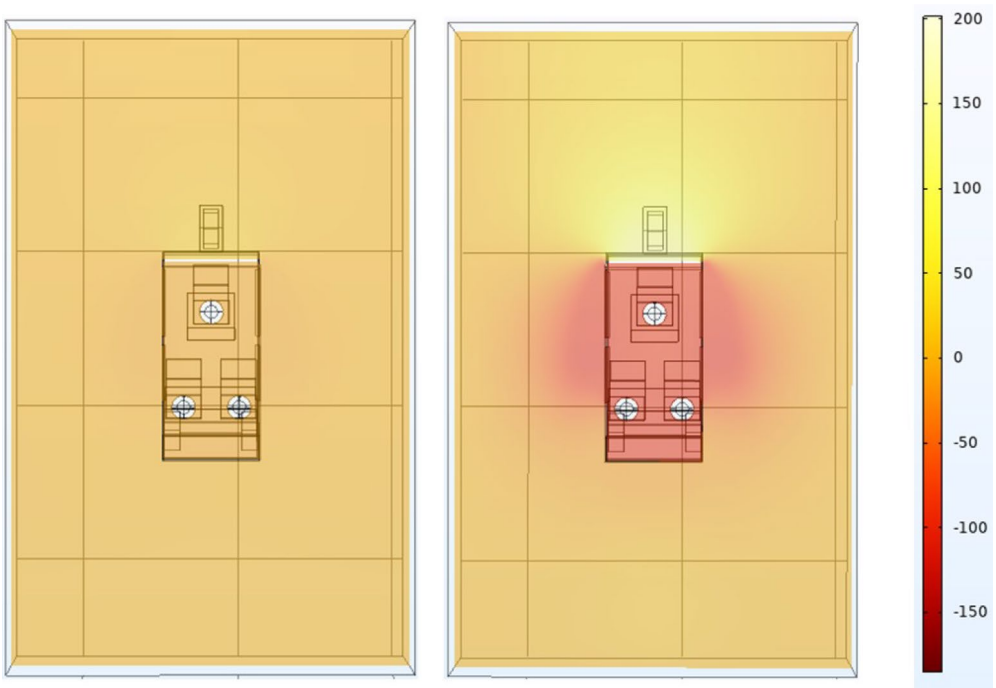

(c) (d)

◂**Fig. 8** **a** Velocity contour with streamlines for auto-rickshaw speed of 20 km/h, **b** velocity contour with streamlines for auto-rickshaw speed of 60 km/h, **c** pressure contour for an auto rickshaw traveling at 20 km/h and **d** pressure contour for an auto rickshaw traveling at 60 km/h. Velocity contour color bar is in m/s while pressure contour color bar is in Pa

Figure 13(a–f) illustrates the spread of particles when there is no partition between the driver's and passengers' compartments.

The results show that when the driver speaks, the ejected particles become entrained in both vortices on either side of the auto-rickshaw enclosure and enter the passenger compartment, exposing both passengers B and C to potential infection. When passenger C speaks, the particles move forward and become entrained in the vortex on the left-hand side. Following the prevailing flow field, the particles enter the driver's compartment but do not pass close to the driver's head, as seen in the side view. This ensures that the driver (A) remains safe. The particles then exit the auto-rickshaw enclosure without affecting passenger B. However, when passenger B speaks, the ejected particles move forward and become trapped in the vortex on the right-hand side. At this stage, a fraction of the particles moves backward and exits the auto-rickshaw enclosure following the prevailing flow field, while another fraction is injected into the vortex on the opposite (left-hand) side, directly across the driver's compartment. As the particles traverse the driver's compartment, they pass very close to the driver's face, putting the driver (A) at risk. However, on their way out, the particles do not pose a threat to passenger C, ensuring that passenger C remains safe.

Table 2 summarizes the infection risk for the other two individuals when one person speaks continuously without a mask.

Hence, it can be observed that when there is no partition between the driver's and passengers' compartments, the risk of infection exists when either the driver or passenger B speaks. However, when a partition is present, the risk of infection arises only when passenger B speaks. Thus, it can be concluded that, overall, the presence of a partition reduces the likelihood of infection. However, such a partition is not a foolproof solution.

Discussion

Probability of spread of infection

In the various scenarios discussed earlier in this paper, when one of the three individuals in the auto rickshaw speaks, the others may or may not be affected. This is determined by whether any particles enter an imaginary cubic enclosure (0.4 m edge length) centered precisely around the spherical head of a passenger. Based on the risk profile, the probability of infection spread for each scenario is estimated. The probability of infection spread is defined as the ratio of the number of individuals at risk when one of the three occupants in the auto rickshaw speaks. For example, in the scenario where the auto rickshaw is traveling at 60 km/h without a partition between compartments, when the driver (person A) speaks, both passengers seated behind (B and C) are exposed to infection. Thus, the probability of infection spread is 1. In contrast, when a partition is present, neither passenger B nor C is affected when the driver (A) speaks, resulting in a probability of infection spread of 0. Table 3 summarizes the probability of infection spread for all the studied cases.

The analysis reveals a significant probability of infection spread in a moving auto rickshaw, with the probability value varying depending on the specific scenario. At this stage, we aim to quantify which of the four scenarios studied has the most significant impact. To achieve this, we calculate the coefficient of variance (COV) in percentage for each of the four parameters examined. The COV for each scenario is defined as the ratio of the standard deviation of the probability of infection spread to its average value over the range of values considered for that scenario. For example, when the vehicle speed increases from 20 to 60 km/h, the probability of infection spread rises from 0 to 1, resulting in a COV of 141.4%. Table 4 presents the coefficient of variance (COV) in percentage for each of the four parameters analyzed.

Among the parameters studied, vehicle speed, the presence of a lateral gust of wind, and the presence of a partition between the driver and passenger compartments are the most influential factors affecting the probability of infection spread. In all three cases, the probability varies from 0 to 1.

To quantify the sensitivity of infection spread probability to these three parameters, we use a sensitivity index (S), as defined by Sen and colleagues (Sen et al. 2024, 2019). The sensitivity index is the ratio of two terms: the numerator represents the ratio of the maximum variation of the tracked parameter to its average value, while the denominator represents the ratio of the maximum variation of the independent parameter to its average value. This approach normalizes the effect of the independent parameter, providing a clearer understanding of its relative influence on infection spread probability.

$$S = \frac{\frac{|y_{max} - y_{min}|}{y_{avg}}}{\frac{x_{max} - x_{min}}{x_{avg}}} \tag{11}$$

Here, y is the probability of spread of infection and x is the value of independent parameters (presence of partition, auto-rickshaw speed, and lateral wind speed).

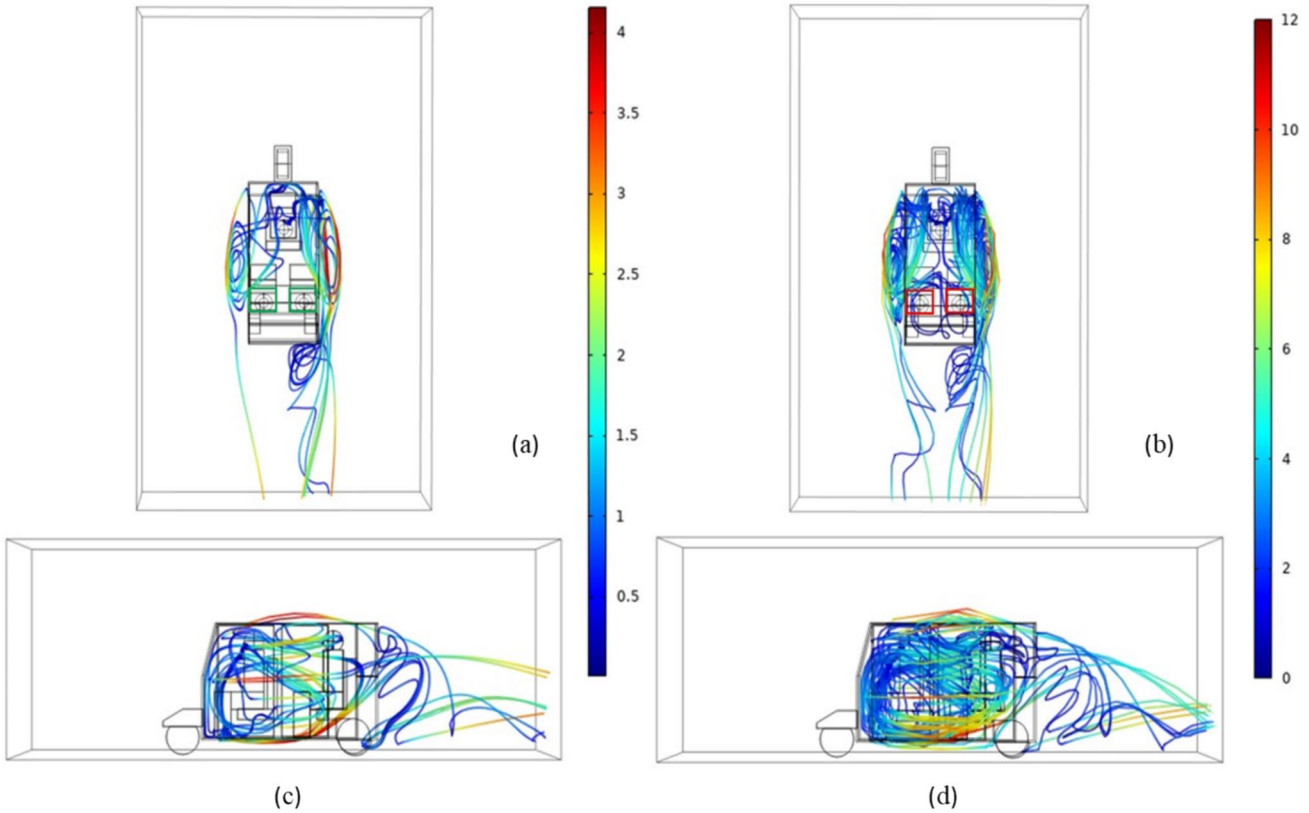

Fig. 9 **a** Top view of aerosol particle tracks for auto rickshaw traveling at 20 km/h, **b** top view of aerosol particle tracks for auto rickshaw traveling at 60 km/h, **c** side view of aerosol particle tracks for auto rickshaw traveling at 20 km/h, and **d** side view of aerosol particle tracks for auto rickshaw traveling at 60 km/h. Color bar represents particle velocity in m/s

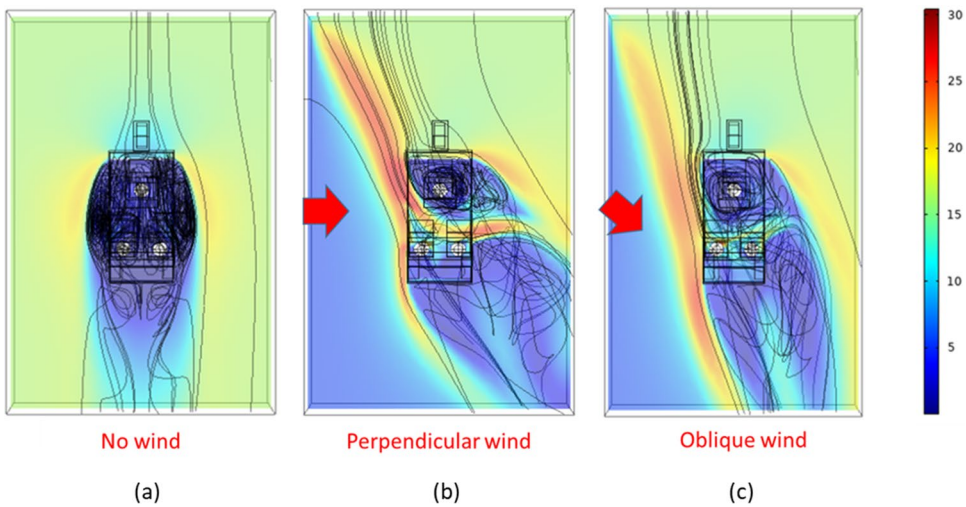

Fig. 10 **a** Velocity contour with streamlines for the case of no lateral wind, **b** perpendicular lateral wind at 20 km/h, and **c** oblique lateral wind at 20 km/h. Auto-rickshaw speed is 60 km/h. Velocity contour color bar is in m/s

In the present study, the sensitivity index (S) for the three independent parameters—presence of a partition between the driver and passenger compartments (0–1), auto-rickshaw speed (20–60 km/h), and lateral wind velocity (0–20 km/h)—is calculated as 1, 2, and 1, respectively. This indicates that auto-rickshaw speed is the most influential factor affecting the probability of infection spread.

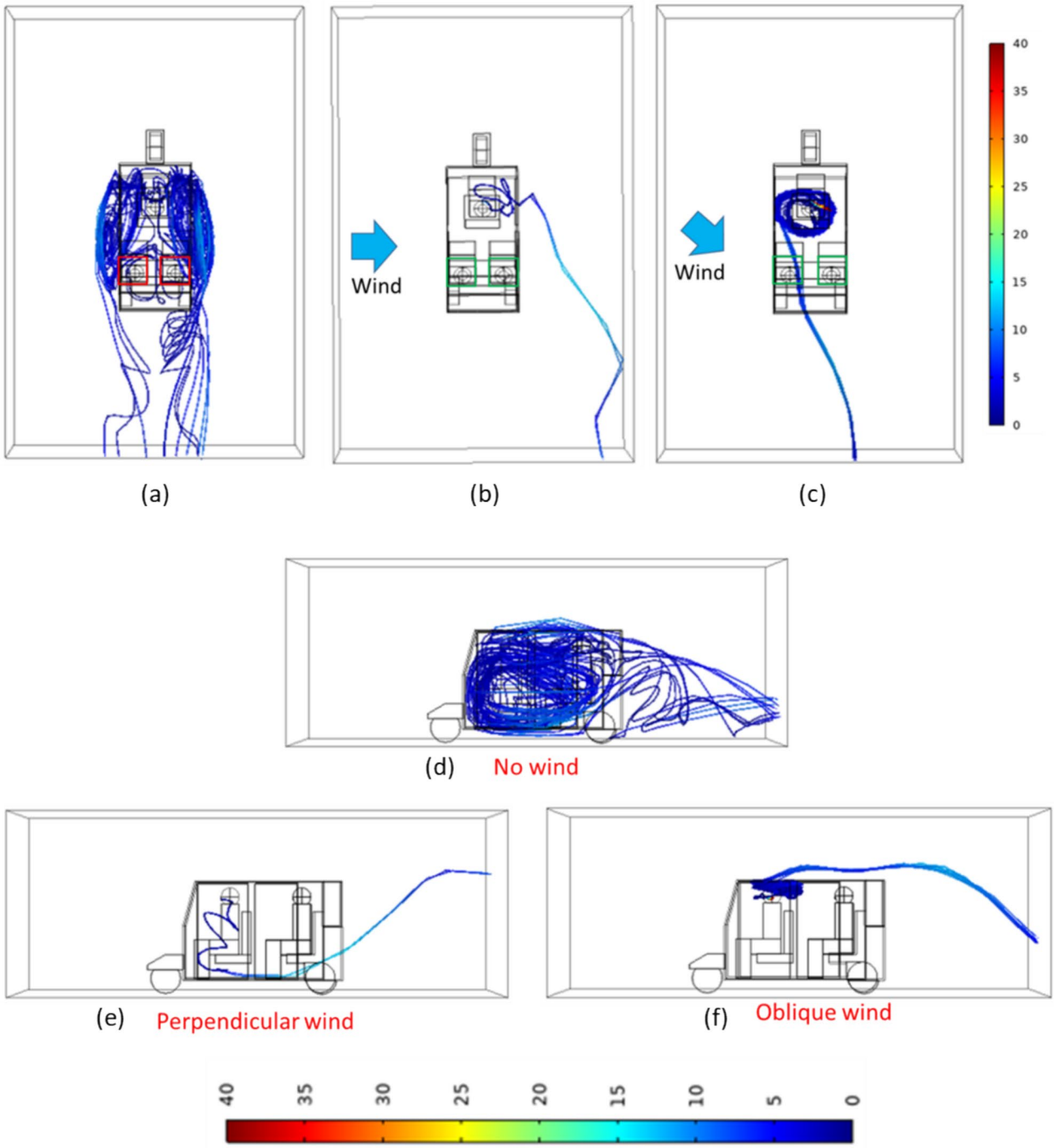

Fig. 11 Top view of aerosol particle tracks for the case of **a** no lateral wind, **b** perpendicular lateral wind at 20 km/h, and **c** oblique lateral wind at 20 km/h. Side view of aerosol particle tracks for the case of **d** no lateral wind, **e** perpendicular lateral wind at 20 km/h, and **f** oblique lateral wind at 20 km/h. Auto-rickshaw speed is 60 km/h. Color bar represents particle velocity in m/s

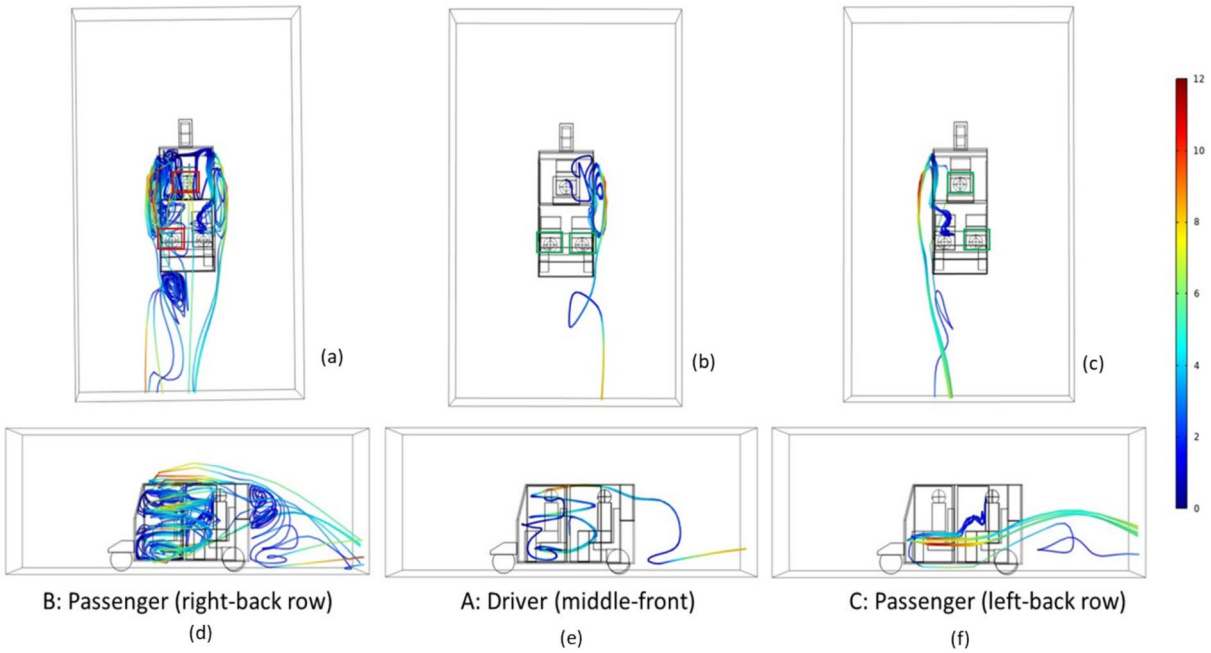

Fig. 12 Top view of aerosol particle tracks for the cases when **a** passenger B, **b** driver, and **c** passenger C speak. Side view of aerosol particle tracks for the cases when **d** passenger B, **e** driver, and **f** passenger C speak. Auto rickshaw traveling at 60 km/h with partition between driver and passenger's compartment. Color bar represents particle velocity in m/s

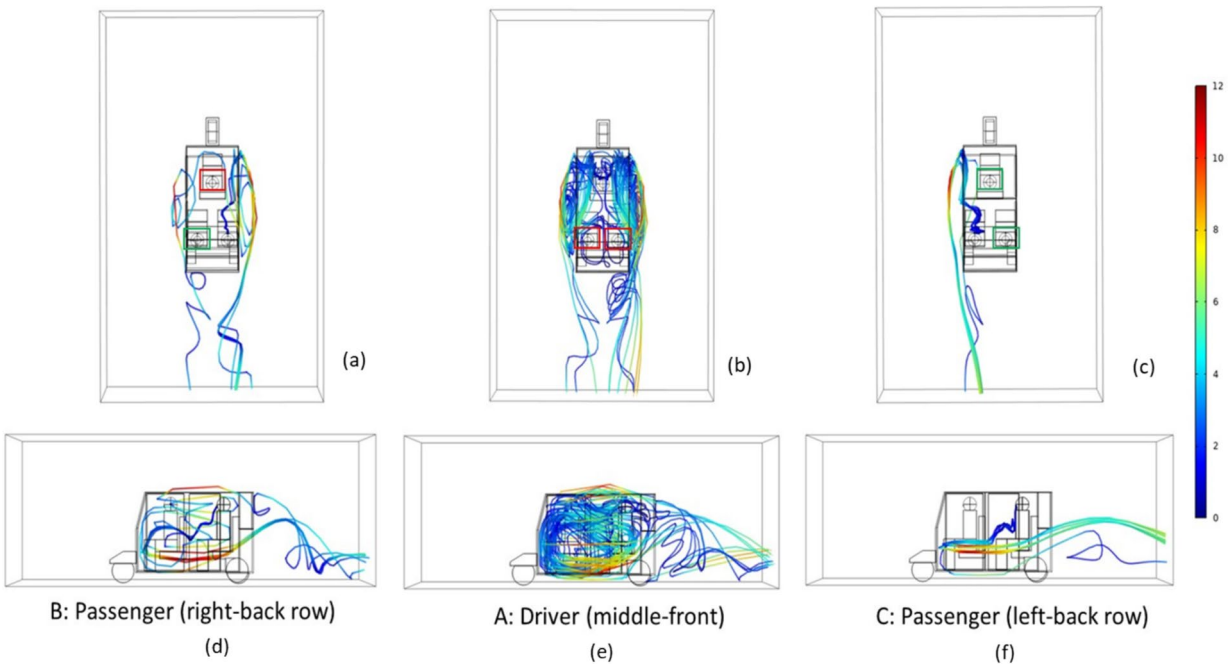

Fig. 13 Top view of aerosol particle tracks for the cases when **a** passenger B, **b** driver, and **c** passenger C speak. Side view of aerosol particle tracks for the cases when **d** passenger B, **e** driver, and **f** passenger C speak. Auto rickshaw traveling at 60 km/h without any partition between driver and passenger's compartment. Color bar represents particle velocity in m/s

Table 2 Risk assessment of different persons seated in an auto rickshaw

	A speaks		B speaks		C speaks	
With partition	B is safe	C is safe	A at risk	C at risk	A is safe	B is safe
Without partition	B at risk	C at risk	A at risk	C is safe	A is safe	B is safe

Table 3 Risk of spread of infection for different scenarios studied

Scenario studied	Vehicle speed (km/h)	Partition between compartments	Source of particles	Lateral wind (km/h)	Number of persons affected	Probability of spread of infection
Effect of partition	60	Yes	A		0	0
	60	No	A		2	1
Effect of vehicle speed	20	No	A		0	0
	60	No	A		2	1
Effect of lateral gust of wind	60	No	A	20, perpendicular	0	0
	60	No	A	20, oblique	0	0
Effect of particle origin source	60	Yes	A		0	0
	60	Yes	B		2	1
	60	Yes	C		0	0
	60	No	A		2	1
	60	No	B		1	0.5
	60	No	C		0	0

Table 4 Relative influence of different scenarios studied

Parameter	Range	Coefficient of variance in probability of spread of infection (%)
Effect of vehicle speed	20–60 km/h	141.42
Effect of partition between driver and passenger compartment	With and without partition (0 or 1)	141.42
Effect of lateral gust of wind	0–20 km/h	141.42
Origin of aerosol particles	Driver (A) or any one of the passengers (B or C)	117.98

Recommendations and comparison with other modes of transport

At this stage, it is essential to summarize the key findings of this study:

1. Vehicle speed: Keeping the speed of the auto rickshaw as low as possible is advisable to minimize the probability of infection spread.
2. Partition between driver and passengers: The presence of a partition between the driver and passenger compartments significantly reduces the risk of infection transmission in a moving semi-open auto rickshaw. It is also a practical and easily implementable solution. However, as shown in Table 2, while it helps mitigate risks, it is not entirely foolproof.
3. Effect of external wind: The worst-case scenario occurs when there is no external wind across the lateral openings of the auto rickshaw. In contrast, the presence of a lateral wind—whether perpendicular or oblique—flushes respiratory particles out of the vehicle, thereby reducing the risk to passengers. This effect is observed even at a modest lateral wind velocity of 20 km/h.
4. Speaker's location: The location of the person speaking also influences the probability of infection spread. For instance, in the absence of a partition, the risk is significantly higher if the driver speaks without a mask.

This study highlights several possible mechanisms of aerosol dispersion inside a moving auto rickshaw and provides general guidelines regarding vehicle speed and the use of partitions. Future research could explore additional scenarios, such as the impact of a zigzag driving pattern, the effect of passengers turning their heads while speaking, or real-time passenger movement. In these cases, the

Table 5 Comparison with reports on other modes of public transport

Reference	Transport mode	Recommendations
El-Salamony et al. 2021	Underground metro wagon (with/without open window) *(Numerical study)*	Opening windows help reduce probability of spread of infection by as much as 40% Increasing ventilation flow rate reduces the probability up to a point beyond which there is no further change Location of source of particles has a strong influence on probability of spread of infection
Mathai et al. 2021	Moving car (4-seater) with 2 seated persons (with/without open window) *(Numerical study)*	Opening windows reduces probability of spread of infection significantly Opening all 4 windows completely minimized chances of spread of infection
Talaat et al. 2021	Boeing 737 airplane *(Numerical study)*	Use of sneeze shield/guards are recommended. Stops transmission of particles 50 µm or larger and reduces transmission of particles in 1–20-µm range Deposition of particles are more on seats/walls than ground
Yang et al. 2020	Air-conditioned long-distance coach bus *(Numerical study)*	Wet air (95% relative humidity) reduces probability of spread of infection (increases deposition rate) Staggered seating (non-adjacent seats) reduce probability of spread Direction of ventilation air supply is important. Supply of ventilation air toward the back of the bus minimized chances of particle (infection) spread
Zhang and Li 2012	Air-conditioned high-speed rail (HSR) cabin *(Numerical study)*	A ventilation mode where there is no continuous flow of air though an inlet but exhaust near the bottom is ideal to minimize probability of spread of infection The placement of luggage rack also has an effect on the airflow patterns in the HSR cabin
Present study	Semi-open auto rickshaw *(Numerical study)*	Lower vehicle speed reduces probability of spread of infection Use of a partition between driver and passenger's compartment reduces probability of spread of infection Location of source of particles has a strong influence on spread probability Gust of external lateral wind helps reduce probability of spread

static mesh approach used in this study would be insufficient, requiring dynamic mesh models (Zhu et al. 2022).

At this point, it is also relevant to compare the findings of this study on aerosol transport in a moving semi-open auto rickshaw with existing literature on other modes of public transport. Table 5 presents a comparison of the key recommendations from this study with those reported for an underground metro wagon with and without open windows (El-Salamony et al. 2021), a moving car with and without open windows (Mathai et al. 2021), an air-conditioned airplane (Talaat et al. 2021), a long-distance air-conditioned coach bus (Yang et al. 2020), and an air-conditioned high-speed railway coach (Zhang and Li 2012).

It can be observed that in air-conditioned modes of transport, the ventilation rate and the direction of airflow have the most significant influence on the fate of respiratory droplets and, consequently, the probability of infection spread. However, in cases where windows can be opened, fully opening them is always beneficial in reducing the risk of infection. Additionally, in most scenarios, the location of the particle source plays a crucial role in determining the risk of infection. For semi-open auto rickshaws, the location of the particle source is also a key factor in assessing the probability of infection spread. The use of a partition between the driver and passenger compartments in an auto rickshaw is comparable to the sneeze shields or guards proposed by Talaat and co-workers (Talaat et al. 2021). While such practical measures are not entirely foolproof, they play a significant role in preventing large-scale infection transmission in public transport systems during a pandemic.

Conclusion

A 3D Euler-Lagrangian CFD model is developed to track the transport and dispersion of aerosol particles generated when a person (either the auto-rickshaw driver or one of the two passengers) speaks unhindered in a moving

auto rickshaw. The model calculates velocity and pressure fields by solving momentum and continuity equations with RANS-based turbulence closure. The Eulerian portion of the model has been extensively validated using reported experimental data on flow fields in an empty cubical enclosure, as well as in a cubical enclosure with an obstacle placed at its center. A grid independence test was conducted to ensure the adequacy of the mesh density used in the simulations. Significant air exchange between the interior and exterior of the auto-rickshaw compartments is observed. The presence of a partition between the driver and passenger compartments reduces the risk of infection spread from 1 to 0, as particles generated in the driver's compartment exit without entering the passenger area. Although this is not a foolproof solution, it is a practical and effective mitigation measure. An increase in auto-rickshaw speed from 20 to 60 km/h increases the probability of infection spread from 0 to 1, highlighting the importance of maintaining a lower vehicle speed. The predicted face velocities at the locations of passengers A, B, and C are 0.45, 0.23, and 0.27 m/s, respectively, for an auto-rickshaw speed of 20 km/h (without a partition). For a speed of 60 km/h (without a partition), the corresponding values increase to 1.40, 0.76, and 0.88 m/s for passengers A, B, and C, respectively. The presence of even a modest lateral wind (20 km/h) significantly reduces the probability of infection spread from 1 to 0. For a perpendicular wind of 20 km/h, the estimated face velocities for passengers A, B, and C are 1.30, 7.55, and 13.22 m/s, respectively. A sensitivity analysis of probability terms indicates that vehicle speed is the most influential factor affecting the probability of infection spread. Finally, a set of recommendations is outlined and compared with those reported for other modes of public transport.

Abbreviations

C_d: Drag coefficient [–]; d_d: Particle diameter [m]; g: Acceleration due to gravity [m s^{-2}]; G_k: Turbulent kinetic energy generation rate [kg m^{-1} s^{-3}]; k: Turbulent kinetic energy [m^2 s^{-2}]; p: Static pressure [Pa]; $\vec{u}$: Velocity vector of air [m s^{-1}]; $\vec{u}_d$: Particle velocity [m s^{-1}

Greek letters

ρ: Density of air [kg m^{-3}]; ρ_d: Particle density [kg m^{-3}]; ε: Turbulent energy dissipation rate [m^2 s^{-3}]; μ: Viscosity of air [Pa s]; μ_T: Turbulent viscosity [Pa s]; $\overline{\overline{\tau}}$: Total stress [Pa

Author contribution Nirvik Sen was involved in conceptualization of different scenarios used in simulations, conducting simulations, model validation, analysis of results, and writing draft manuscript. Krishna Kumar Singh was involved in conceptualization of different scenarios used in simulations, checking the analysis and results, and correcting the manuscript.

Funding Open access funding provided by Department of Atomic Energy. The authors declare that no funds, grants, or other support were received during the preparation of this manuscript.

Data availability The data that support the findings of this study are available from the authors upon reasonable request.

Declarations

Ethics approval We conform that we have adhered to strict profession ethics while preparing the work reported.

Consent to participate We confirm that the study does not involve participation of any human or animal subject.

Consent to publish We confirm that all co-authors of this work have provided consent to publish the work.

Conflict of interest The authors declare no competing interests.

References

Abuhegazy M, Talaat K, Anderoglu O, Poroseva SV (2020) Numerical investigation of aerosol transport in a classroom with relevance to COVID-19. Phys Fluids 32(10):103311

Baker S, Fang X, Shen L, Willman C, Fernandes J, Leach F, Davy M (2023) Dynamic mode decomposition for the comparison of engine in-cylinder flow fields from particle image velocimetry (PIV) and Reynolds-Averaged Navier-Stokes (RANS) simulations. Flow Turbul Combust 111:115–140

Dbouk T, Drikakis D (2020a) On coughing and airborne droplet transmission to humans. Phys Fluids 32:053310. https://doi.org/10.1063/5.0011960

Dbouk T, Drikakis D (2020b) On respiratory droplets and face masks. Phys Fluids 32:063303. https://doi.org/10.1063/5.0015044

Elmaghraby HA, Chiang YW, Aliabadi AA (2020) Airflow design and source control strategies for reducing airborne contaminant exposure in passenger aircraft cabins during the climb leg. Sci Technol Built Environ 26(7):901–903

El-Salamony M, Moharam A, Guaily A, Boraey MA (2021) Air change rate effects on the airborne diseases spreading in underground metro wagons. Environ Sci Pollut Res 28:31895–31907

Horikiri K, Yao Y (2011) Validation study of convective airflow in an empty room. In: 2nd INEEE Conference: Energy, Environment, Devices, Systems, Communications, Computers (EEDSCC '11); 2011 (March 7-10), Venice, Italy

Horita N, Fukumoto T (2023) Global case fatality rate from COVID-19 has decreased by 96.8% during 2.5 years of the pandemic. J Med Virol, 95(1). https://doi.org/10.1002/jmv.28231

Ji Y, Qian H, Ye J, Zheng X (2018) The impact of ambient humidity on the evaporation and dispersion of exhaled breathing droplets: a numerical investigation. J Aerosol Sci 115:164–172

Li X, Shang Y, Yan Y, Yang L, Tu J (2018) Modelling of evaporation of cough droplets in inhomogeneous humidity fields using the multi-component Eulerian-Lagrangian approach. Build Environ 128:68–76

Liu L, Wei J, Li Y, Ooi A (2017) Evaporation and dispersion of respiratory droplets from coughing. Indoor Air 27:179–190

Liu H, He S, Shen L, Hong J (2021) Simulation-based study of COVID-19 outbreak associated with air-conditioning in a restaurant. Phys Fluids 33(2):023301

Liu J, Hao M, Chen S, Yang Y, Li J, Mei Q, Bian X, Liu K (2022) Numerical evaluation of face masks for prevention of COVID-19 airborne transmission. Environ Sci Pollut Res 29(29):44939–44953

Mathai V, Das A, Bailey JA, Breuer K (2021) Airflows inside passenger cars and implications for airborne disease transmission. Sci Adv 7(1):eabe0166. https://doi.org/10.1126/sciadv.abe0166

Mboreha CA, Jianhong S, Yan W, Zhi S (2022) Airflow and contaminant transport in innovative personalized ventilation systems for aircraft cabins: a numerical study. Sci Technol Built Environ 28(4):557–574

Narayanan SR, Yang S (2021) Airborne transmission of virus-laden aerosols inside a music classroom: effects of portable purifiers and aerosol injection rates. Phys Fluids 33(3):033307

Sarhan AAR, Naser P, Naser J (2022) Numerical study of when and who will get infected by coronavirus in passenger car. Environ Sci Pollut Res 29(38):57232–57247

Saw LH, Leo BF, Nor NSM, Yip CW, Ibrahim N, Hamid HHA, Latif MT, Lin CY, Nadzir MSM (2021) Modeling aerosol transmission of SARS-CoV-2 from human-exhaled particles in a hospital ward. Environ Sci Pollut Res 28(38):53478–53492

Sen N (2021) Transmission and evaporation of cough droplets in an elevator: numerical simulations of some possible scenarios. Phys Fluids 33:033311

Sen N, Singh KK (2021a) When the doorbell rings in COVID-19 times: numerical insights into some possible scenarios. Phys Fluids 33:045128

Sen N, Singh KK (2021b) Spread of virus laden aerosols inside a moving sports utility vehicle with open windows: a numerical study. Phys Fluids 33(9):095117

Sen N, Singh KK, Mukhopadhyay S, Shenoy KT (2019) Drop formation at a hole in a plate submerged in quiescent continuous phase: comparison of plain hole and nozzle hole. Chem Eng Commun 206(10):1317–1336

Sen N, Badiwal A, Singh KK, Mukhopadhyay S, Shenoy KT (2024) Optimization of bromocresol green degradation using ozone micro bubbles: response surface analysis and techno-commercial aspects of a 75 kL/day scale-up plant. Discov Environ 2(1):48

Song Y, Yang C, Li H, Chen H, Shen S, Hou Y, Wang J (2023) Aerodynamic performance of a ventilation system for droplet control by coughing in a hospital isolation ward. Environ Sci Pollut Res 30(29):73812–73824

Talaat K, Abuhegazy M, Mahfoze OA, Anderoglu O, Poroseva SV (2021) Simulation of aerosol transmission on a Boeing 737 airplane with intervention measures for COVID-19 mitigation. Phys Fluids 33:033312

Tan H, Wong KY, Othman MHD, Kek HY, Wahab RA, Ern GKP, Chong WT, Lee KQ (2022) Current and potential approaches on assessing airflow and particle dispersion in healthcare facilities: a systematic review. Environ Sci Pollut Res 29(53):80137–80160

Wang M, Chen Q (2009) Assessment of various turbulence models for transitional flows in an enclosed environment (RP-1271). Hvac&r Res 15(6):1099–1119

Wang C, Liu B, Zhang S, Huang N, Zhao T, Lu QB, Cui F (2023) Differences in incidence and fatality of COVID-19 by SARS-CoV-2 Omicron variant versus Delta variant in relation to vaccine coverage: a world-wide review. J Med Virol 95(1):e28118

Won Y, Rim D, Mistrick R, Bahnfleth W (2023) CFD modeling of room airflow effects on inactivation of aerosol SARS-CoV-2 by an upper-room ultraviolet germicidal irradiation (UVGI) system. Sci Technol Built Environ 29(7):719–729

Wong SC, Au AKW, Chen H, Yuen LLH, Li X, Lung DC, Chu AWH, Ip JD, Chan WM, Tsoi HW, To KKW (2022) Transmission of Omicron (B. 1.1. 529)-SARS-CoV-2 variant of concern in a designated quarantine hotel for travelers: a challenge of elimination strategy of COVID-19. Lancet Reg Health-West Pac 18:100360

Worldometer (2023) see https://www.worldometers.info/coronavirus/forCoronavirusCases. Accessed Oct 2024

Xu C, Wang J, Yu L, Sui X, Wu Q (2023) Omicron Subvariant BA.5 is highly contagious but containable: successful experience from Macau. Front Public Health 10:1029171

Yang X, Ou C, Yang H, Liu L, Song T, Kang M, Lin H, Hang J (2020) Transmission of pathogen-laden expiratory droplets in a coach bus. J Hazard Mater 397:122609

Zhang L, Li Y (2012) Dispersion of coughed droplets in a fully-occupied high-speed rail cabin. Build Environ 47:58–66

Zhu C, Peng C, Wu W, Wang C (2022) A multi-layer SPH method for generic water–soil dynamic coupling problems. Part I: Revisit, theory, and validation. Comput Methods Appl Mech Eng 396:115106